Article

Current Biology

Biological Motion as an Innate Perceptual Mechanism Driving Social Affiliation

Graphical Abstract

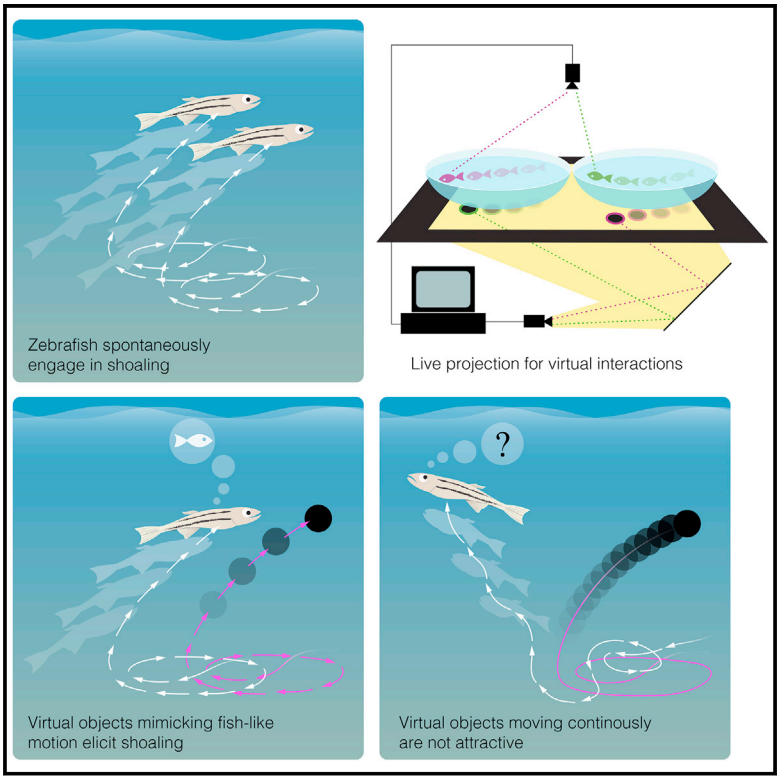

Authors

Johannes Larsch, Herwig Baier

Correspondence

hbaier@neuro.mpg.de

In Brief

Fundamental sensory cues driving collective behavior remain elusive because dynamically interacting animals present an intertwined choreography where stimulus-response relationships are unclear. Larsch and Baier analyze zebrafish interactions with virtual objects and identify biological motion as a potent trigger of social affiliation.

Highlights

- Juvenile zebrafish affiliate with black dots that mimic zebrafish motion
- Developing fish gradually match their kinetic preference to age-specific motion
- Social affiliation does not require reciprocal attraction
- Motion cues alone can induce age-assortative shoaling

Larsch & Baier, 2018, Current Biology *28*, 3523–3532
November 19, 2018
https://doi.org/10.1016/j.cub.2018.09.014

CellPress

Current Biology
Article

CellPress

Biological Motion as an Innate Perceptual Mechanism Driving Social Affiliation

Johannes Larsch[1] and Herwig Baier[1,2,*]
[1]Max Planck Institute of Neurobiology, Department Genes - Circuits - Behavior, Am Klopferspitz 18, D-82152 Martinsried, Germany
[2]Lead Contact
*Correspondence: hbaier@neuro.mpg.de
https://doi.org/10.1016/j.cub.2018.09.014

SUMMARY

Collective behavior, such as shoaling in teleost fish, is driven by the perceptual recognition of conspecific animals. Because social interactions are mutual, it has been difficult to disentangle the exact sensory cues that trigger affiliation in the first place from those that are emitted by receptive and responsive shoal mates. Here, we overcome this challenge in a virtual reality assay in zebrafish. We discovered that simple visual features of conspecific biological motion provide a potent shoaling cue. Individual juvenile fish shoal for hours with circular black dots projected onto a screen, provided these virtual objects mimic the characteristic kinetics of zebrafish swim bouts. Other naturalistic cues previously implicated in shoaling, such as fish-like shape, pigmentation pattern, or non-visual sensory modalities are not required. During growth, the animals' stimulus preferences shift gradually, matching self-like kinetics, and this tuning exists even in fish raised in isolation. Virtual group interactions and our multi-agent model implementation of this perceptual mechanism demonstrate that kinetic cues can drive assortative shoaling, a phenomenon commonly observed in field studies. Coordinated behavior can emerge from autonomous interactions, such as collective odor avoidance in *Drosophila*, or from reciprocal interactions, such as the codified turn-taking in wren duet singing. We found that individual zebrafish shoal autonomously without evidence for a reciprocal choreography. Our results reveal individual-level, innate perceptual rules of engagement in mutual affiliation and provide experimental access to the neural mechanisms of social recognition.

INTRODUCTION

Social interactions are essential to animals for survival and reproduction, suggesting that dedicated neuronal circuits exist to process socially relevant information [1–3]. Indeed, specific groups of neurons in flies, mice, and primates exert causal roles on social tasks such as social recognition, affiliation, mating, and aggression [4–6]. Neuromodulators such as oxytocin, serotonin, and tachykinin regulate these behaviors across species and provide striking examples of evolutionary conservation in the control of social interactions, highlighting the potential of studying fundamental social principles in model organisms [4, 5, 7].

Social behaviors are triggered and regulated by conspecific cues, and identifying their precise nature is central to social neuroscience. The best understood examples of such cues are pheromones that control innate behaviors via streamlined olfactory circuits [4, 8, 9]. In *Drosophila melanogaster*, for example, the pheromone 11-cis-vaccenyl acetate activates olfactory sensory neurons which express the olfactory receptor Or67d. Output from Or67d neurons triggers sex-specific changes in mating behavior via sexually dimorphic connections with brain regions such as the lateral horn [9]. In comparison, much less is known about fundamental visual cues despite the fact that vision is required for many social behaviors including collective motion in groups [10], particularly in humans where the importance of pheromones is unclear [8]. Studies on display behavior in cichlids and face processing in primates provide just a glimpse of socially relevant visual cues awaiting discovery [1, 11, 12]. One major challenge to analyzing vision during social interactions is the dynamic, intermingled nature of visual cues exchanged by interacting animals. This hampers a systematic analysis of stimulus-response relationships and each animal's causal contribution to the joint behavior, particularly in animal groups engaged in collective behavior such as swarm coordination [3, 13, 14]. Quantitative descriptions of freely moving fish shoals, bird flocks, and human crowds provide evidence that formation and maintenance of intraspecific groups are governed by a small number of simple behavioral rules, such as long-distance attraction and short-distance repulsion among individuals [3, 10, 15–17]. However, the challenge of isolating the fundamental visual cues and perceptual processes driving collective behavior remained unsolved and prevented dissecting the mechanistic implementation of collective rules at the level of neural circuits.

A powerful model of collective behavior is zebrafish shoaling, a form of affiliation with conspecifics that facilitates predator avoidance, foraging, and stress coping [3, 18, 19]. Mutual attraction among zebrafish develops between 10 to 20 days of age, when an increasing fraction of swim steering events become socially biased toward neighboring fish and animals maintain a preferred distance from one another [17, 20, 21]. Previously, sensory triggers of shoaling were analyzed in adult fish by recording the location of a focal individual relative to one or several test fish separated by a transparent vertical divider. Such experiments revealed that individual animals were more attracted toward larger groups than toward single animals and preferred

pigmentation types experienced during early development [22, 23]. More recently, analysis of adult zebrafish responding to semi-realistic fish images on computer screens or biomimetic replica revealed effects of stimulus size, color, shape, and motion on attraction [14, 24]. Together, these results paint a complex picture of multiple interacting cues without any one visual feature dominating attraction. Bridging the gap between shoaling rules inferred from freely moving animals and attraction toward stimuli across a divider requires dynamic stimulus presentation and analysis of unrestrained interactions with artificial stimuli. Such experiments become feasible through the advent of closed-loop stimulus presentation and observer-centric virtual reality techniques [25, 26]. In this study, we use a virtual-reality setup to present dynamic social stimuli to freely swimming animals at elevated throughput for psychophysical analysis in comparison to natural shoaling with real conspecifics. We find that kinetics features representing fish-like biological motion in the absence of photorealistic fish-like appearance trigger persistent shoaling. We analyze shoaling of developing juvenile animals over a range of kinetic stimulus parameters and find an age-specific preference for self-like motion. By comparing mutual interactions between fish to interactions with non-interactive stimuli and simulated interactions in a multi-agent model, we propose that individuals shoal autonomously without reciprocal dialog. Together, these results outline perceptual principles of social recognition and provide a starting point to analyze the organization of neural circuits controlling collective behavior.

RESULTS

Virtual Interactions Driven by Cross-Projected Interactive Dots

To investigate social affiliation, we tracked pairs of fish freely swimming in shallow dishes (Figure 1A). Under such conditions, zebrafish readily engage in shoaling [20]. Figure 1B shows an example of two juvenile fish (26 days post-fertilization [dpf]) spontaneously following each other closely over almost the entire observation period of 20 min. The inter-animal distance (IAD, 5–20 mm) is well below the average distance expected from chance encounters (40 mm) (Figure 1B), a hallmark of shoaling [20]. We defined attraction as the percent reduction in mean IAD relative to control IAD expected by chance; this index was highly significant in each of 7 pairs at this age (Figure 1B). In control experiments, we found that fish swimming individually in vertically stacked transparent dishes were still attracted to one another, indicating that vision provides sufficient sensory cues for shoaling (Figure S1A). Vision was also required: upon turning off all visible light, animals separated within seconds to chance level IAD (Figure S1B).

These findings prompted us to devise a simple virtual reality shoaling assay to reveal the fundamental visual cues that drive shoaling. We placed fish in separate dishes above a projection screen onto which we cross-projected in real time a black dot at the location of another fish (Figures 1A and S1E). This dot virtually links two physically separated fish and was therefore termed "interactive". Notably, it enables mutual interactions in the absence of visual detail such as body shape, pigmentation, tail motion, depth, or texture—cues that were previously implicated in regulating shoaling [14, 24, 25]. Pairs readily interacted via interactive dots of 3.7 mm diameter (Figure 1B and Video S1); their attraction was on average 87% of physical attraction measured in the same animals (physical: 0.65 ± 0.06 SD; virtual: 0.56 ± 0.08 SD. Figure 1B). The strength of attraction increased sharply with age and was correlated between physical and virtual conditions from 17–26 days of age, suggesting that both assays probe a related behavior that matures during this time (Figure 1C). Shoaling is a persistent behavior of zebrafish in the wild [19]. Accordingly, physical and virtual attraction were maintained over a 12 hr period and fell only toward the evening (Figure 1D), demonstrating persistent engagement of the animals with interactive dots.

Onset of shoaling occurs at around 2 weeks of age [20, 21], a period of rapid development in zebrafish, including a doubling in body length from 4 mm to 8 mm within 2 weeks [27] and a gradual transition from well-isolated swim bouts to near-continuous swimming [27, 28] (Figure S2). To dissociate the roles of increased social drive and animal size on mutual attraction during animal growth, we modulated the dot diameter from 0.9 mm to 7.5 mm and recorded virtual interactions in 70 pairs from 10–27 dpf (Figures 1E–1G). From 14 dpf, an increasing fraction of pairs showed attraction to 3.7 mm dots, reaching 100% of pairs at 19 dpf (Figure 1E). Attraction was strongest to dots of diameters of 1.8 and 3.7 mm, with a trend for older animals to prefer larger dots (Figure 1F). These sizes correspond to the parts of a juvenile zebrafish that provide the highest contrast such as the head, torso, and the eyes (Figure 1F).

Natural shoaling is explained in part by two behavioral rules: long-range attraction and short-range repulsion together result in characteristic animal spacing [3, 17]. Neighborhood maps representing the likelihood of finding a neighbor in space reveal a time average of these opposing behaviors [16]. We compared neighborhood maps of virtually versus physically interacting animals with respect to this signature. Physically interacting animals less than 14 dpf mainly exhibited repulsion and attraction was increasingly prominent in older animals (Figure 1G). Maps of virtually interacting animals were most similar to physical interaction at dot sizes of 1.8 to 3.7 mm with a ring of attraction around a central zone of repulsion (Figures 1G and S2). Short-range repulsion from the most attractive stimuli indicates that dot stimuli trigger shoaling behavior rather than pursuit of potential prey. From these results, we conclude that a circular black dot, which interactively mirrors the position of another animal, can induce shoaling.

Fish-like Stimulus Kinetics Trigger Attraction toward Passive-Attractive Dot Stimuli

Next, we sought to understand the minimal motion parameters that render a dot stimulus attractive to induce shoaling. Object speed is a key stimulus feature in hunting and escape behavior [29–31], suggesting that dot speed might also regulate social affiliation. Alternatively, animals might extract higher-order motion parameters such as acceleration or path curvature. For example, acceleration oscillates once every swim bout because propulsion and gliding alternate at about 1–2 Hz [28], a kinetic signature of biological motion [32] in zebrafish, which may be used to detect conspecifics.

To address these possibilities, we measured individual animals' attraction to dots moving along a set of synthetic stimulus

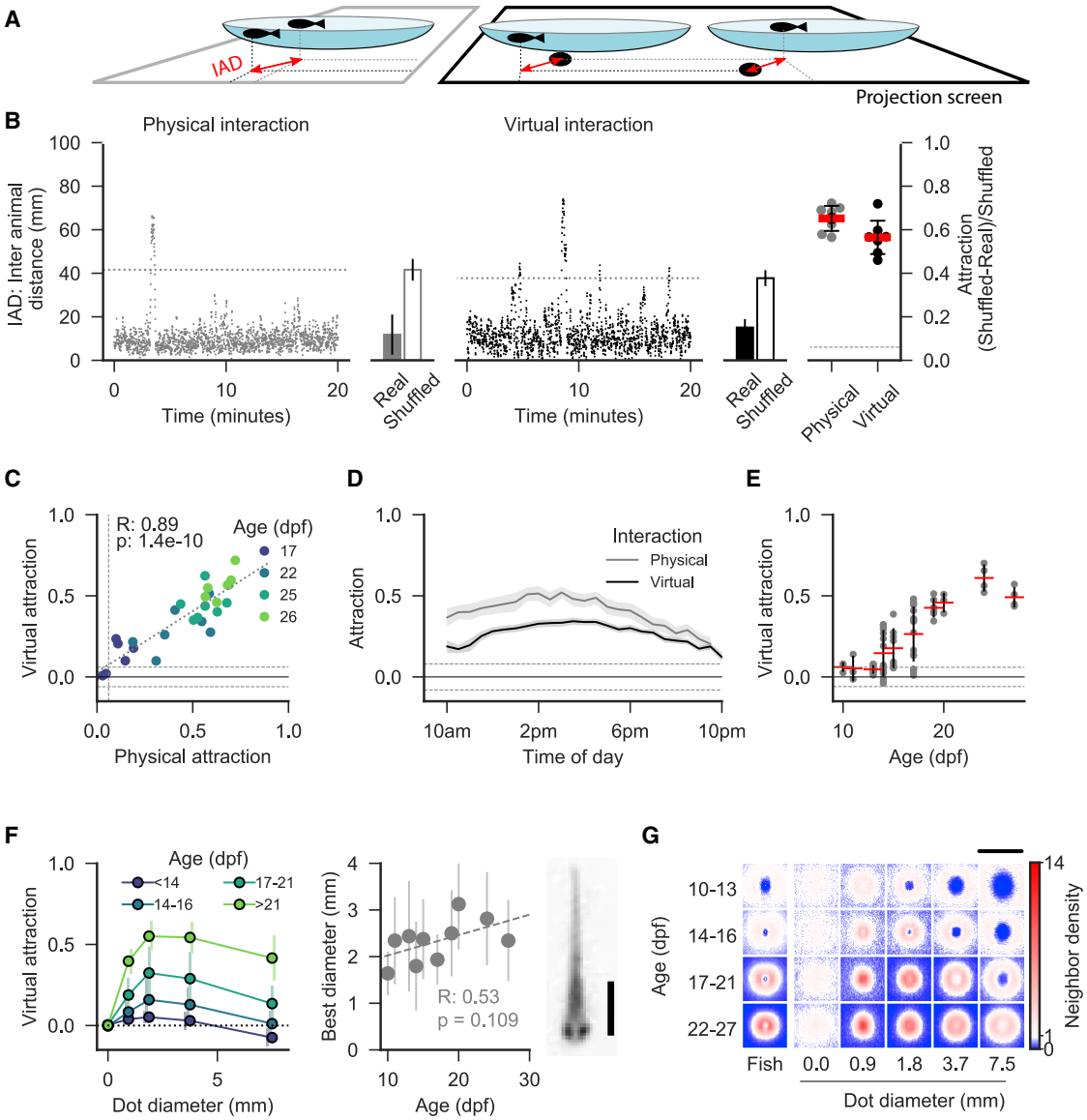

Figure 1. Virtual Interactions Driven by Cross-Projected Interactive Dots

(A) Schematic of experiments: Two animals interact physically (left) or virtually (right) in a watch glass of 10 cm diameter. In the virtual condition, a black dot is projected onto a screen below each dish at the location of the animal in the other dish. Double arrows indicate dot-animal distance or inter animal distance (IAD).

(B) Representative IAD traces for one pair tested successively in both interaction modes. Bar graphs indicate mean ± 1 SD of real IAD_r over 120 min for these animals versus chance level IAD_s obtained by time shuffling the position data. Right: An attraction index is calculated as $(IAD_s\text{-}IAD_r)/IAD_s$. Age: 26 dpf. Data points indicate individual pairs, red bars indicate mean ± 1 SD, 120 min data per pair. Dashed line: 95% confidence interval (CI) for h_0 of no attraction, see STAR Methods and Figure S1 for detail.

(C) Attraction in individual pairs correlates between interaction modes across age. n = 7 pairs per age group. 120 min data per animal.

(D) Attraction persists throughout the day. Traces represent mean during 29 min bins, shading represents 95% CI over animals. n = 14 pairs (physical), 21 pairs (virtual), age: 23–25 dpf.

(E) Attraction in the virtual mode increasingly exceeds 95% CI for no attraction between 2–3 weeks of age. Dot size = 3.8 mm. Data points represent individual pairs, >40 min data per animal. Red bars indicate mean at each age ± 1 SD. n = 70 pairs.

(F) Dot diameter modulates attraction. Left, data points represent mean attraction for four age groups. Dot sizes were 0, 0.9, 1.8, 3.7, 7.5 mm. Right, data points represent mean of the most attractive dot diameter over animals at each age ± 1 SD. Dashed line represent linear fit through the mean values. Same data as (E). Image shows a 21 dpf animal. Scale bar: 2 mm.

(G) Neighbor density distribution during physical interactions with another animal (left) and virtual interactions via black dots of variable diameter (right). A focal fish defines the center of each map. Red and blue color indicate higher and lower probability than chance, respectively, of finding the neighbor animal at a given location. Maps are mean probability over multiple animals. Physical interaction data (Fish) are the same as in (C). Virtual interaction data are the same as in (E). Scale bar represents 60 mm. See also Figure S1 and S2 and Video S1.

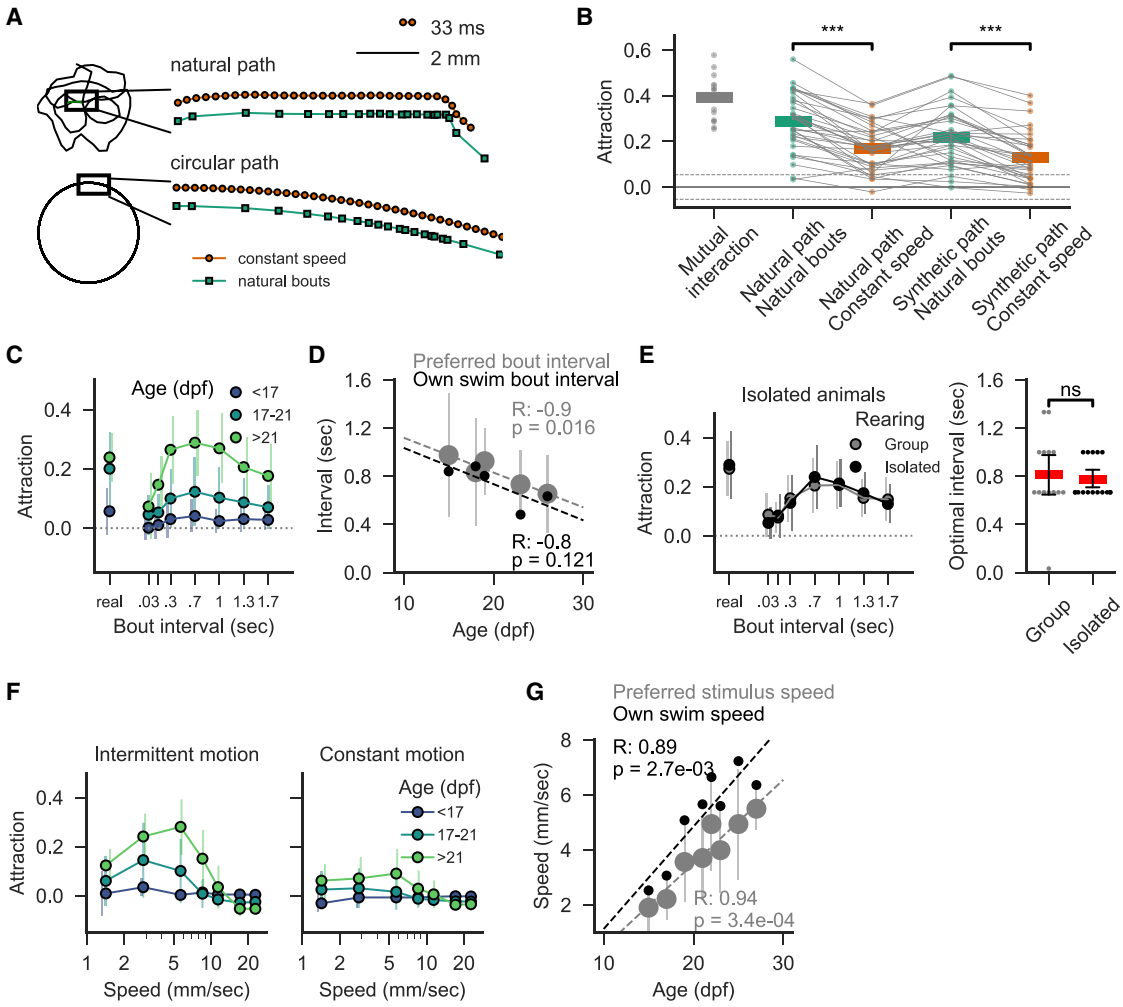

Figure 2. Fish-like Stimulus Kinetics Trigger Attraction toward Passive-Attractive Dot Stimuli

(A) Schematic of stimulus paths and kinetics: Colored data points indicate dot position in consecutive frames (33 ms). Constant speed paths were generated by interpolating natural paths while maintaining average speed.

(B) Natural bout kinetics render dot stimuli attractive. n = 36 animals, 21–30 dpf. Dashed line: 95% confidence interval (CI) for h_0 of no attraction. ***: significant at $p < 0.001$. Dunn's multiple comparisons test for matched samples following ANOVA Friedman test, $p < 0.0001$. Gray lines connect individuals across stimuli. See Table S1 for all pairwise comparisons.

(C) Attraction to dots moving intermittently along a knot-shaped path. Bout interval was varied at fixed average speed of 5.7 mm/sec. "Real" denotes attraction to a dot moving on a natural path with natural bouts. Data points represent mean attraction over animals at each age group ± 1 SD. n = 15–30 animals per age group.

(D) Optimal bout interval (gray) tracks age-specific spontaneous swim bout frequency (black). Data represent mean of most attractive bout interval over animals at each age. Error bars are 1 SD. Dashed lines represent linear fit through group means. Same data as (C).

(E) Rearing animals in isolation does not affect overall attraction or optimal interval at 18 dpf. Data are mean ± 1 SD. n = 14, 16 group, isolated. NS = not significant: Mann-Whitney test $p > 0.5$.

(F) Constant speed stimuli (update interval = 33 ms) yield low attraction at all speeds. Intermittent motion stimuli (update interval = 666 ms) are most attractive at speeds that parallel natural swim speed across age 15-27 dpf. Data points represent mean ± 1 SD.

(G) Gray data points represent mean of most attractive dot speed over animals at each age ± 1 SD. Black data points represent average swim speed in the absence of a stimulus, n = 15–30 animals per age group. Dashed lines represent best linear fit through group means. See also Figure S2 for correlations of age with speed and bout frequency, Video S2 and Figure S3.

paths that dissociated swim kinetics and swim paths by replacement with circular paths and constant speed, respectively (Figure 2A). Such dots were non-interactive, moved identically for each animal and were, hence, called 'passive-attractive'. Fish also followed passive-attractive dots allowing us to quantify individual's unilateral attraction (Figure 2B; Video S2). We noticed a preference for dot movement with natural swim kinetics over movement at constant speed that was largely independent of the dot path (Figure 2B, Table S1), suggesting that fish recognize swim kinetics as a sign stimulus [11] for social affiliation.

Next, we decomposed natural swimming by simplifying its bout structure. We measured attraction toward dots moving in discontinuous jumps (bouts) over a range of intervals from continuous to intermittent bout-like motion at a fixed average

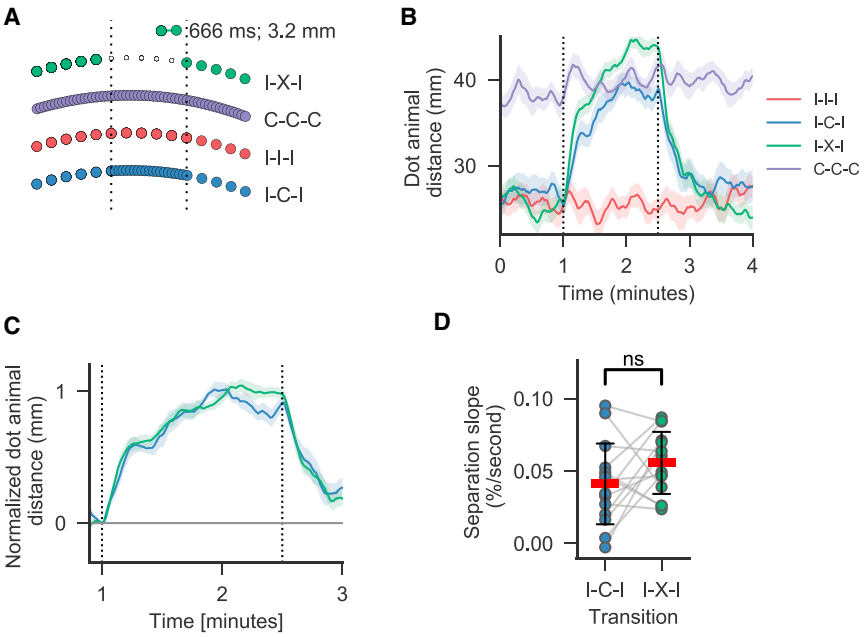

Figure 3. Rapid Evaluation of Social Attractiveness

(A) Dot attractiveness is modulated at transitions from intermittent motion (I: 666 ms update rate) to constant speed (C: 33 ms update rate) or an invisible dot (X). The four stimulus conditions last 6 min each (4 min shown) and repeat in randomized order for 8 hr. The invisible dot disappears for 90 s but is analyzed as if moving at constant speed along the same path as a visible dot.

(B) Dot-animal distance reaches a steady state within 1 min after the transition (dashed lines). This separation represents a combination of a change in attraction and drift toward a new steady state. Lines represent mean distance, shading represents 95% CI, n = 14 animals, 20–23 dpf.

(C) Same data as B, normalization highlights similarity of the time courses.

(D) Slope of dot-animal distance during 10 s after stimulus transition. NS: not significant, related samples t test $p > 0.15$. See also Figure S4 for individual animal dot-animal distance.

speed. Attraction was strongly regulated by bout interval from 0.03 s to 1.3 s (Figure 2C). We detected a negative correlation of the preferred bout interval with age: it ranged from 0.97 ± 0.51 s to 0.65 ± 0.32 s between 15 - 27 dpf, closely tracking the fish's own spontaneous swim bout frequency at each age (Figure 2D). Strikingly, the overall attraction and age-specific optimal bout interval of fish reared in isolation was similar to control animals raised in groups (Figure 2E). This indicates that an innate mechanism underlies the development of stimulus pattern recognition.

To ask how speed modulates attraction, we presented fish with intermittent and continuous motion at average speeds of 1.5–24 mm/s. Intermittent motion was more attractive at all speeds (Figure 2F), and attraction dropped sharply at speeds above 10 mm/s. The preferred dot speed rose from 2–6 mm/s between 15 and 27 dpf, again tracking the animal's own spontaneous swim speed (Figure 2G). In contrast, continuous motion was ineffective at all speeds, as was inverting dot contrast to light on dark (Figure S3). This tuning to self-like motion is further evidence that virtual interactions represent social affiliation.

Rapid Evaluation of Social Attractiveness

Next, we sought to reveal the timescale on which fish integrate visual information when judging dot attractiveness. Juvenile zebrafish perform swim maneuvers on a sub-second timescale, resulting in rapidly fluctuating IAD time series of individual pairs (see Figure 1B). This observation inspired us to analyze IAD with passive attractive dots on a frame-by-frame basis while changing dot kinetics (Figure 3A). At one extreme, animals might adjust attraction levels as soon as stimulus kinetics change, observable as a sudden change in IAD. In a different scenario, animals might display persistent or gradually decaying attraction for a limited time. For example, animals might continue to follow a dot that was switched from intermittent to continuous motion as if it was still moving intermittently. This would manifest as a delayed or slowed change in IAD. On average, fish had low steady-state IAD during intermittent motion and high IAD during continuous motion (Figure 3B). After a transition from intermittent motion to continuous motion, IAD detectably rose in under 5 s and approached the higher steady-state within 1 min (Figures 3B and S4). The increase in IAD potentially reflects a combination of two processes: (i) the animal re-evaluating the stimulus to a lower level of attractiveness, potentially with memory of stimulus history that might cause persistent attraction; (ii) random diffusion-like transition to the higher steady-state IAD for continuous dot motion at a rate that depends on swim speed and arena geometry.

To isolate the rate of stimulus re-evaluation, we compared separation from a dot transitioned from intermittent motion to continuous motion (I-C-I) versus separation from a dot turned invisible for 90 s. Invisible dots were also considered to move continuously for the purpose of IAD quantification (I-X-I). Animals effectively do not receive updates on stimulus position for invisible dots and, as a consequence, cannot actively maintain low IAD once the dot disappears. Thus, the increase in IAD during I-X-I transition exclusively represents the random process. Animals separated at similar rates from invisible or continuously moving dots (Figure 3B) and normalizing IAD time series of separation to account for different steady-state levels rendered the time series and rates of change indistinguishable (Figure 3C, 3D, and S4). This implies that juvenile zebrafish evaluate kinetic attractiveness and adjust steering decisions on a timescale of seconds.

Individual Social Drive Predicts Mutual Interactions

A fundamental challenge in analyzing mutual interactions is dissecting each individual's contribution. For example, mutual attraction within a pair and an individual's apparent sociability may be determined by each individual's social drive toward the partner, by each individual's attractiveness as evaluated by the

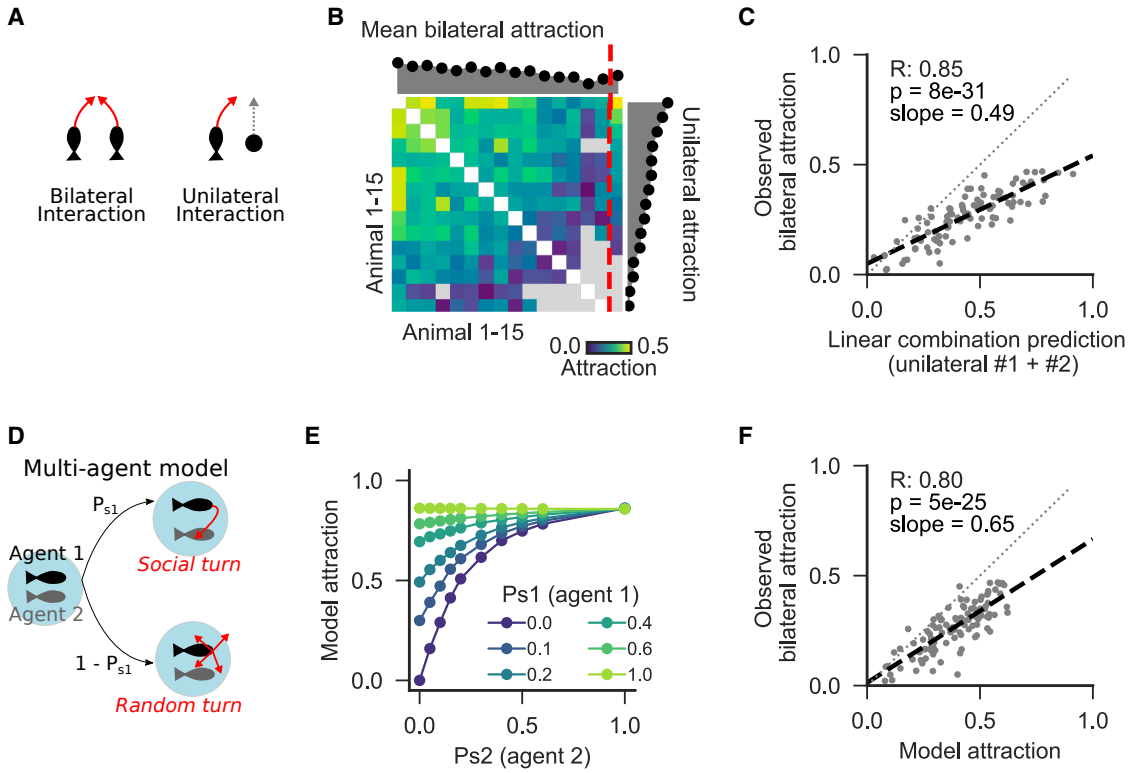

Figure 4. Individual Social Drive Predicts Bilateral Interactions

(A) Both animals potentially contribute social drive and attractiveness to mutual attraction observed in bilateral interaction. A single animal's social drive determines observed attraction during unilateral interactions.

(B) 15 animals (21 dpf) are sequentially linked for bilateral interactions via interactive dots in all possible 105 pairwise combinations. Each animal is also exposed to a passive-attractive dot moving intermittently to measure unilateral interaction. Rightmost column separated by red dashed line and histogram right represent unilateral attraction and determines plot order. Colors represent mean attraction for each pair over six repeated trials (5 min each). Gray indicates attraction below 95% CI (0.09). Histogram above indicates column-wise mean attraction. See also Figure S4D.

(C) Pairwise bilateral attraction is predicted as the sum of the two individuals' unilateral attraction. Each data point represents one of 105 possible pairings. Dashed line is linear fit through data. Dotted line is unity.

(D) Schematic of multi-agent model inspired by Hinze et al. [20]. Agent n turns toward other agents with social turn probability P_{sn} or into a random direction with probability 1-P_{sn}. Agent speed, bout rate, arena size and simulated frame rate match our data.

(E) Mutual attraction between agents varies with social turn parameter P_{sn}. P_{s1} = 0 corresponds to unilateral attraction of agent 2.

(F) The model predicts observed bilateral attraction using P_{sn} parameters inferred from unilateral interactions. Each dot represents one of 105 models using P_{sn} parameters corresponding to the animal pairs in (C). Dashed line represents unity.

partner, or by a combination of these two. In addition, mutual interactions may require explicit reciprocity with the partner—for example, in the form of codified turn-taking as observed in duet singing in wrens. During zebrafish shoaling, synchronization of swim bouts between neighbors [21] may provide a cue to boost attraction in a synergistic manner when such reciprocity is detected. To ask if individual's social drive increases with reciprocating partners, we sequentially measured bilateral attraction within all possible 105 virtual pairings of 15 animals via interactive dots. In each animal, we also measured unilateral attraction toward a passive-attractive dot (Figures 4A and 4B). Unilateral attraction is not confounded by the individual's attractiveness but instead is a direct reflection of social drive. Unilateral attraction of individuals and bilateral attraction within specific pairs were repeatable across trials but varied substantially between animals (Figures 4B and S4D). Mutual attraction of individuals to other animals was correlated across pairings, resulting in a range of mean bilateral attraction (MBA), reflecting apparent sociability of individual animals from effectively non-social to highly social (Figure 4B).

We found that unilateral attraction correlated with MBA (R = 0.91, Figure 4B), implying that mainly social drive, and not attractiveness, determines mutual interactions and, thus, apparent sociability in our data. We could therefore predict bilateral attraction for each pair as the linear sum of each individual's unilateral attraction (Figure 4C).

Next, we sought to further understand effects of individual's social drive and a potential role for reciprocity on pair-level measurements of IAD and attraction. To this end, we built a multi-agent NetLogo [33] model, implementing a simple attraction rule [20] controlled by a social drive parameter (Figure 4D). In a multi-agent model, individuals are modeled as agents that interact with a virtual environment and with each other according to user-defined rules at each simulated time step. Such models have been used extensively to explore interaction rules underlying collective behaviors [15].

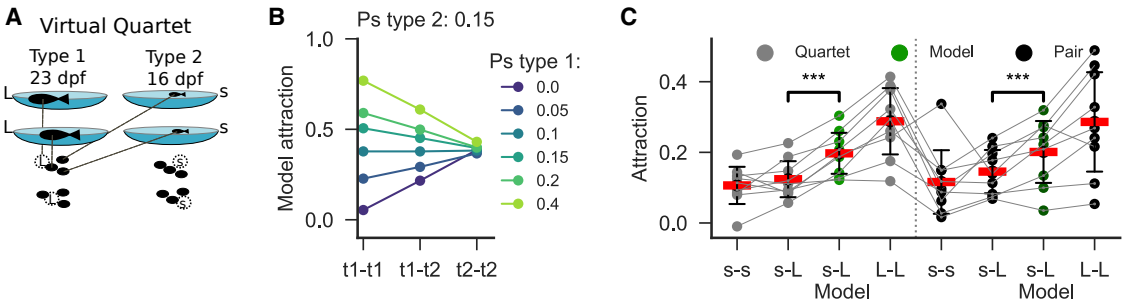

Figure 5. Motion Cues Induce Age-Assortative Shoaling

(A) Schematic of a virtual quartet consisting of two animals each of two types (s: small = 16 dpf and L: large = 23 dpf). Each animal sees black dots underneath at the location of the other three animals. All dots are of the same size. Interspersed are time periods where the same animals are virtually linked in pairs.

(B) Multi-agent model for quartet of 2 types differing only in P_{sn} predicts attraction between types (t1-t2) as the mean of attraction within types.

(C) Attraction between types (s-L) was lower than predicted by the model (green). This preference was similar when tested simultaneously in a quartet or separately in pairs. Data points represent mean attraction over 4-6 repeated trials. Note that quartet interactions were analyzed and plotted pairwise: s-L attraction represents mean over the four possible s-L combinations. Red bars indicate group means ± 1SD. n = 9 × 4 animals. Gray lines connect repeated-measures of the same pair. ***$p < 0.001$, related samples t test. See also Figure S5.

The virtual arena was modeled as a circle of 100 mm diameter, and agents moved at constant speed of 6 mm/s, calculating 30 updates per simulated 1 s modeled time, closely matching our experimental conditions (Figure S2). Agents move forward at each step and make a turn once per second. This effectively ties steering events to the frequency of swim bouts, a simplification justified by the observation that swim trajectories of larval zebrafish consist of straight segments interspersed with high angle turns at swim bouts [28].

To focus our analysis on the effect of individual's social drive on attraction, we followed previous work [20] and implemented only one simple attraction rule, ignoring other proposed interaction rules such as short-range repulsion or alignment of agents.

Turn direction of agent n is controlled by the following rule:

1. Social turn: with probability P_{sn} turn toward the center of mass of all other agents in the arena, or,
2. Random turn: with probability 1 - P_{sn} turn to a random direction.

Thus, P_{sn} dictates the fraction of socially driven turns, a parameter proposed to mature during the ontogeny of zebrafish shoaling [20].

To simulate the effect of an individual's social drive on mutual attraction (Figure 4E), we repeatedly ran the model for 72,000 steps (40 min simulated time) using different sets of P_{s1} and P_{s2} for two agents, respectively. Attraction increased with P_s of both agents and reached a plateau at 0.85 attraction (Figure 4E). The curve for $P_{s1} = 0$ represents unilateral attraction of agent 2 because agent 1 was effectively asocial (Figure 4E). This curve allows to infer P_s for each animal in Figure 4B based on observed unilateral attraction.

Next, we evaluated how closely our model matches observed mutual attraction. We used the inferred values of P_s for the 15 animals in Figure 4B to create 105 combinations of P_{s1} and P_{s2} for the model. Model attraction was highly correlated with observed bilateral attraction using these parameters (R = 0.80, Figure 4F). Importantly, this model does not explicitly implement synergies in mutually interacting pairs. Thus, juvenile zebrafish did not distinguish between interactive versus passive-attractive dots. We conclude that individuals autonomously evaluate conspecific motion as a shoaling stimulus mainly as a function of their own social drive.

Motion Cues Induce Age-Assortative Shoaling

Field observations of fish shoals commonly describe affiliation preferences for conspecifics and size-matched animals [3]. Such assortative shoaling can help individuals to evade detection by confusing predators who may target rare phenotypes, a form of selective predation also known as the oddity effect [3]. To ask how differences in social drive and preferences for specific motion kinetics might act to sort larger groups, we analyzed virtually interacting quartets composed of two younger, weakly social fish (16 dpf) and two older, strongly social fish (23 dpf) (Figure 5A). Each animal saw three dots of equal size at the position of the other fish. This configuration discards stimulus size as a factor influencing affiliation but retains age-specific stimulus kinetics. To test for affiliation preferences within a quartet, we calculated pairwise attraction within and between the age groups. As predicted, we found weakest and strongest attraction within the young and old groups, respectively, and intermediate inter-group attraction (Figure 5C). To assess if the observed inter-group attraction reflects a preference for age-specific kinetics, we returned to the multi-agent model and predicted inter-group attraction in the absence of age-specific kinetic preferences. To this end, groups of four agents were simulated, each agent belonging to one of two types. The types differed only in p_{sn}. We repeatedly ran the model, varying p_{s1} while keeping p_{s2} constant. We found that inter-group attraction was always the mean of intra-group attraction for all combinations of p_{s1} and p_{s2} tested (Figure 5B). We therefore predict inter-group attraction as precisely the mean of intra-group attraction for all quartets of real animals (Figure 5C). However, inter-group attraction was lower than predicted by this simple model (Figure 5C). This result is consistent with active selection of preferred stimulus kinetics among multiple stimuli. To ask if indirect effects of different swim kinetics can explain assortative shoaling [34], we

extended the model to implement group differences in swim speed, bout interval and an explicit within-group preference as a proxy for kinetic preferences. Of these parameters, only explicit within-group preference reproduced the observed affiliation preference (Figure S5). For comparison, we also analyzed attraction in the same animals when virtually linked into the six possible pairs of each quartet for pairwise interaction. Attraction within and across age groups was similar between pairs versus quartet in the same animals, demonstrating that the presence of two additional stimuli neither confuses nor enhances the animal's preferences for motion kinetics (Figure 5C). From these results, we conclude that age-specific differences in motion cues provide sufficient sensory information to induce assortative shoaling.

DISCUSSION

Until now, sensory cues implicated in shoaling were numerous, and their link to naturally unfolding behavior was unclear. Our results suggest that the perceptual basis of shoaling is simpler than previously thought. We discovered that the social "instinct" [11] of zebrafish is released by visual features of the swim kinetics of another zebrafish. Imposing the bout structure typical of a juvenile fish on the movement of a projected, two-dimensional dot in a virtual reality arena elicited shoaling behavior that resembled physical interactions with respect to its ontogeny, strength of affiliation, and relative animal spacing.

Biological motion is a potent releaser of intraspecific and interspecific interactions in fish [35, 36], birds [37], and mammals including humans [38], and impaired interpretation of biological motion has emerged as an early heritable marker for autism [39, 40]. In human psychophysics, biological motion typically refers to motion of body parts relative to each other, which is readily recognized by humans, even when the position of each limb is indicated only as a dot on a light point display [32]. While naturalistically moving dot arrangements still represent a complex stimulus, local detection of acceleration that is consistent with biological agents emerges as one fundamental 'life-detector' evaluating such stimuli [38]. Our results suggest that a related detector functions as a core perceptual mechanism whose activation readily drives persistent shoaling in zebrafish.

Social cues often elicit innate behaviors, and social experience can profoundly shape such innate responses, providing insights into mechanisms of development and plasticity. One powerful manipulation, for example, is social isolation. In mice, solitary males, but not socially housed males, launch attacks on intruder animals [41]. In contrast to this modulation, we found in juvenile zebrafish that affiliation and tuning to self-like motion exist even after complete social isolation, suggesting an innate developmental mechanism. This raises the possibility that individuals match visual cues against a cognitive representation of idiosyncratic, self-like biological motion which might be generated from proprioceptive feedback or an efference copy of swimming. Alternatively, the visual system might generate a gradually developing motion template independent of self-motion.

Coordinated behavior can emerge from autonomous interactions, such as collective odor avoidance in *Drosophila*, where mechanosensory interactions upon animal collisions enhance the response probability to escape from mildly noxious stimuli [42]. Social interactions can also require explicit reciprocity, such as the codified turn-taking in wren duet singing, which is reflected in neural encoding of the jointly produced song by each individual [43]. We demonstrate persistent attraction of individual juvenile zebrafish toward non-interactive stimuli. Naturally, the observed affiliation of two agents that both move toward each other is closer than affiliation observed between one individual and a non-interactive agent. Within-animal comparisons of bilateral and unilateral interactions together with our multi-agent model suggest that individuals equally shoal with passive-attractive and interactive stimuli. We conclude that juvenile zebrafish autonomously evaluate and respond to motion cues during shoaling rather than coordinating an explicitly reciprocal behavior. This lack of reciprocity suggests that simple passive-attractive stimuli may suffice to activate neural circuits for social processing in restrained animals during functional imaging.

Our analysis revealed consistent variability in mutual attraction between animal pairs which we assigned largely to differences in individuals' responsiveness to motion cues, the social drive of each animal. Recent studies specifically focused on inter-individual differences in repeated-measurements of behavior to reveal genetic and neural causes of phenotypic variability [40, 44, 45] and its effect on collective behavior [34]. It will be important to analyze individual animals over longer periods of time to determine persistence and heritability of different social personality types. We speculate that individual differences in the perception of motion cues partially predict social drive, consistent with impaired interpretation of biological motion in children with autism [39]. In addition, internal states set by neuromodulatory systems shape behavioral individuality [44, 45]. Differences across these domains are, in principle, detectable at the level of neural activity and provide exciting opportunities to study mechanistic causes and social consequences of phenotypic diversity.

Defining minimal visual social cues in a genetic model organism opens the door for future studies on the underlying brain mechanisms analogous to the discovery of pheromones and their role in shaping animal behavior [4, 8, 9]. Our results provide a baseline set of stimuli at the earliest social stage to which juvenile zebrafish likely add as they mature. Future work in older animals will reveal developmental stages when other naturalistic cues such as the conspicuous zebrafish pigmentation gain influence on shoaling decisions. In the meantime, our stimulus provides a clear path forward for identifying those areas in the zebrafish brain tuned to biological motion stimuli displayed to restrained animals during functional imaging of whole brain activity and optogenetic interrogation [46–48]. Our finding that changes to stimulus kinetics control attraction within seconds suggests that neural representations of stimulus quality can be analyzed using simple stimulus protocols. It will be interesting to trace the neural pathways that underpin the social instinct from the detection of conspecifics by the visual system to the innate responses encoded in the hypothalamic and limbic centers of the forebrain [49]. Since social affiliation is a common feature across the vertebrate taxon, the core principles of neural architecture are likely to be conserved from fish to human.

STAR★METHODS

Detailed methods are provided in the online version of this paper and include the following:

- KEY RESOURCES TABLE
- CONTACT FOR REAGENT AND RESOURCE SHARING
- EXPERIMENTAL MODEL AND SUBJECT DETAILS
- METHOD DETAILS
- QUANTIFICATION AND STATISTICAL ANALYSIS
  - Multi-agent Model
- DATA AND SOFTWARE AVAILABILITY

SUPPLEMENTAL INFORMATION

Supplemental Information includes five figures, one table, and two videos and can be found with this article online at https://doi.org/10.1016/j.cub.2018.09.014.

A video abstract is available at https://doi.org/10.1016/j.cub.2018.09.014#mmc5.

ACKNOWLEDGMENTS

We thank Marco Dal Maschio and Joseph Donovan for help with designs for the setup and statistics. We thank X. Jin, S.W. Flavell, D. Ventimiglia, S.J. Rahi, A. Tallafuss, P. Washbourne, and members of the Baier laboratory for comments on the manuscript and discussions. Funding was provided by the Max Planck Society.

AUTHOR CONTRIBUTIONS

J.L. and H.B. conceived the study. J.L. designed and conducted experiments and analyzed the data. J.L. and H.B. interpreted the data and wrote the paper.

DECLARATION OF INTERESTS

The authors declare no competing interests.

Received: June 20, 2018
Revised: August 13, 2018
Accepted: September 10, 2018
Published: November 1, 2018

REFERENCES

1. Fernald, R.D. (2012). Social control of the brain. Annu. Rev. Neurosci. *35*, 133–151.
2. Stanley, D.A., and Adolphs, R. (2013). Toward a neural basis for social behavior. Neuron *80*, 816–826.
3. Krause, J., and Ruxton, G.D. (2002). Living in Groups (OUP Oxford).
4. Bergan, J.F. (2015). Neural Computation and Neuromodulation Underlying Social Behavior. Integr. Comp. Biol. *55*, 268–280.
5. Anderson, D.J. (2016). Circuit modules linking internal states and social behaviour in flies and mice. Nat. Rev. Neurosci. *17*, 692–704.
6. Sadagopan, S., Zarco, W., and Freiwald, W.A. (2017). A causal relationship between face-patch activity and face-detection behavior. eLife *6*, https://doi.org/10.7554/eLife.18558.
7. Garrison, J.L., Macosko, E.Z., Bernstein, S., Pokala, N., Albrecht, D.R., and Bargmann, C.I. (2012). Oxytocin/vasopressin-related peptides have an ancient role in reproductive behavior. Science *338*, 540–543.
8. Liberles, S.D. (2014). Mammalian pheromones. Annu. Rev. Physiol. *76*, 151–175.
9. Auer, T.O., and Benton, R. (2016). Sexual circuitry in Drosophila. Curr. Opin. Neurobiol. *38*, 18–26.
10. Strandburg-Peshkin, A., Twomey, C.R., Bode, N.W.F., Kao, A.B., Katz, Y., Ioannou, C.C., Rosenthal, S.B., Torney, C.J., Wu, H.S., Levin, S.A., and Couzin, I.D. (2013). Visual sensory networks and effective information transfer in animal groups. Curr. Biol. *23*, R709–R711.
11. Tinbergen, N. (1951). The study of instinct (Clarendon Press).
12. Freiwald, W.A., Tsao, D.Y., and Livingstone, M.S. (2009). A face feature space in the macaque temporal lobe. Nat. Neurosci. *12*, 1187–1196.
13. Orger, M.B., and de Polavieja, G.G. (2017). Zebrafish Behavior: Opportunities and Challenges. Annu. Rev. Neurosci. *40*, 125–147.
14. Abaid, N., Bartolini, T., Macrì, S., and Porfiri, M. (2012). Zebrafish responds differentially to a robotic fish of varying aspect ratio, tail beat frequency, noise, and color. Behav. Brain Res. *233*, 545–553.
15. Couzin, I.D., Krause, J., James, R., Ruxton, G.D., and Franks, N.R. (2002). Collective memory and spatial sorting in animal groups. J. Theor. Biol. *218*, 1–11.
16. Katz, Y., Tunstrøm, K., Ioannou, C.C., Huepe, C., and Couzin, I.D. (2011). Inferring the structure and dynamics of interactions in schooling fish. Proc. Natl. Acad. Sci. USA *108*, 18720–18725.
17. Marques, J.C., Lackner, S., Félix, R., and Orger, M.B. (2018). Structure of the Zebrafish Locomotor Repertoire Revealed with Unsupervised Behavioral Clustering. Curr. Biol. *28*, 181–195.
18. Oliveira, R.F., and Faustino, A.I. (2017). Social information use in threat perception: Social buffering, contagion and facilitation of alarm responses. Commun. Integr. Biol. *10*, e1325049.
19. Parichy, D.M. (2015). Advancing biology through a deeper understanding of zebrafish ecology and evolution. eLife *4*, https://doi.org/10.7554/eLife.05635.
20. Hinz, R.C., and de Polavieja, G.G. (2017). Ontogeny of collective behavior reveals a simple attraction rule. Proceedings of the National Academy of Sciences, 201616926.
21. Dreosti, E., Lopes, G., Kampff, A.R., and Wilson, S.W. (2015). Development of social behavior in young zebrafish. Front. Neural Circuits *9*, 39. http://www.frontiersin.org/Article/10.3389/fncir.2015.00039/abstract.
22. Pritchard, V.L., Lawrence, J., Butlin, R.K., and Krause, J. (2001). Shoal choice in zebrafish, *Danio rerio*: the influence of shoal size and activity. Anim. Behav. *62*, 1085–1088.
23. Engeszer, R.E., Ryan, M.J., and Parichy, D.M. (2004). Learned social preference in zebrafish. Curr. Biol. *14*, 881–884.
24. Gerlai, R. (2017). Animated images in the analysis of zebrafish behavior. Curr. Zool. *63*, 35–44.
25. Stowers, J.R., Hofbauer, M., Bastien, R., Griessner, J., Higgins, P., Farooqui, S., Fischer, R.M., Nowikovsky, K., Haubensak, W., Couzin, I.D., et al. (2017). Virtual reality for freely moving animals. Nat. Methods *14*, 995–1002.
26. Dunn, T.W., Gebhardt, C., Naumann, E.A., Riegler, C., Ahrens, M.B., Engert, F., and Del Bene, F. (2016). Neural Circuits Underlying Visually Evoked Escapes in Larval Zebrafish. Neuron *89*, 613–628.
27. Parichy, D.M., Elizondo, M.R., Mills, M.G., Gordon, T.N., and Engeszer, R.E. (2009). Normal table of postembryonic zebrafish development: staging by externally visible anatomy of the living fish. Dev. Dyn. *238*, 2975–3015.
28. Fuiman, L.A., and Webb, P.W. (1988). Ontogeny of routine swimming activity and performance in zebra danios (Teleostei: Cyprinidae). Anim. Behav. *36*, 250–261.
29. Semmelhack, J.L., Donovan, J.C., Thiele, T.R., Kuehn, E., Laurell, E., and Baier, H. (2014). A dedicated visual pathway for prey detection in larval zebrafish. eLife *3*, https://doi.org/10.7554/eLife.04878.
30. Barker, A.J., and Baier, H. (2015). Sensorimotor decision making in the zebrafish tectum. Curr. Biol. *25*, 2804–2814.
31. Temizer, I., Donovan, J.C., Baier, H., and Semmelhack, J.L. (2015). A Visual Pathway for Looming-Evoked Escape in Larval Zebrafish. Curr. Biol. *25*, 1823–1834.

32. Johansson, G. (1973). Visual perception of biological motion and a model for its analysis. Percept. Psychophys. *14*, 201–211.
33. Wilensky, U. (1999). NetLogo. http://ccl.northwestern.edu/netlogo/. Center for Connected Learning and Computer-Based Modeling, Northwestern University. Evanston, IL.
34. Jolles, J.W., Boogert, N.J., Sridhar, V.H., Couzin, I.D., and Manica, A. (2017). Consistent Individual Differences Drive Collective Behavior and Group Functioning of Schooling Fish. Curr. Biol. *27*, 2862–2868.
35. Nakayasu, T., and Watanabe, E. (2014). Biological motion stimuli are attractive to medaka fish. Anim. Cogn. *17*, 559–575.
36. Matsunaga, W., and Watanabe, E. (2012). Visual motion with pink noise induces predation behaviour. Sci. Rep. *2*, 219.
37. Vallortigara, G., and Regolin, L. (2006). Gravity bias in the interpretation of biological motion by inexperienced chicks. Curr. Biol. *16*, R279–R280.
38. Thornton, I.M. (2018). Stepping into the genetics of biological motion processing. Proc. Natl. Acad. Sci. USA *115*, 1687–1689.
39. Klin, A., Lin, D.J., Gorrindo, P., Ramsay, G., and Jones, W. (2009). Two-year-olds with autism orient to non-social contingencies rather than biological motion. Nature *459*, 257–261.
40. Wang, Y., Wang, L., Xu, Q., Liu, D., Chen, L., Troje, N.F., He, S., and Jiang, Y. (2018). Heritable aspects of biological motion perception and its covariation with autistic traits. Proc. Natl. Acad. Sci. USA *115*, 1937–1942.
41. Yang, T., Yang, C.F., Chizari, M.D., Maheswaranathan, N., Burke, K.J., Jr., Borius, M., Inoue, S., Chiang, M.C., Bender, K.J., Ganguli, S., and Shah, N.M. (2017). Social Control of Hypothalamus-Mediated Male Aggression. Neuron *95*, 955–970.e4.
42. Ramdya, P., Lichocki, P., Cruchet, S., Frisch, L., Tse, W., Floreano, D., and Benton, R. (2015). Mechanosensory interactions drive collective behaviour in *Drosophila*. Nature *519*, 233–236.
43. Fortune, E.S., Rodríguez, C., Li, D., Ball, G.F., and Coleman, M.J. (2011). Neural mechanisms for the coordination of duet singing in wrens. Science *334*, 666–670.
44. Pantoja, C., Hoagland, A., Carroll, E.C., Karalis, V., Conner, A., and Isacoff, E.Y. (2016). Neuromodulatory Regulation of Behavioral Individuality in Zebrafish. Neuron *91*, 587–601.
45. Stern, S., Kirst, C., and Bargmann, C.I. (2017). Neuromodulatory Control of Long-Term Behavioral Patterns and Individuality across Development. Cell *171*, 1649–1662.e10.
46. Baier, H., and Scott, E.K. (2009). Genetic and optical targeting of neural circuits and behavior–zebrafish in the spotlight. Curr. Opin. Neurobiol. *19*, 553–560.
47. Feierstein, C.E., Portugues, R., and Orger, M.B. (2015). Seeing the whole picture: A comprehensive imaging approach to functional mapping of circuits in behaving zebrafish. Neuroscience *296*, 26–38.
48. Vanwalleghem, G.C., Ahrens, M.B., and Scott, E.K. (2018). Integrative whole-brain neuroscience in larval zebrafish. Curr. Opin. Neurobiol. *50*, 136–145.
49. Stednitz, S.J., McDermott, E.M., Ncube, D., Tallafuss, A., Eisen, J.S., and Washbourne, P. (2018). Forebrain Control of Behaviorally Driven Social Orienting in Zebrafish. Curr. Biol. *28*, 2445–2451.
50. Lopes, G., Bonacchi, N., Fraz, Ã., £o, J., Neto, J.P., Atallah, B.V., Soares, S., Moreira, L., Matias, S., Itskov, P.M., Correia, P.A., et al. (2015). Bonsai: an event-based framework for processing and controlling data streams. Front. Neuroinform *9*, https://doi.org/10.3389/fninf.2015.00007.
51. Pérez-Escudero, A., Vicente-Page, J., Hinz, R.C., Arganda, S., and de Polavieja, G.G. (2014). idTracker: tracking individuals in a group by automatic identification of unmarked animals. Nat. Methods *11*, 743–748.

STAR★METHODS

KEY RESOURCES TABLE

REAGENT or RESOURCE	SOURCE	IDENTIFIER
Deposited Data		
Raw Behavioral data	This paper	https://doi.org/10.6084/m9.figshare.6939923
Experimental Models: Organisms/Strains		
Wild type TL	NA	ZFIN: ZDB-GENO-990623-2
Software and Algorithms		
Custom Social Behavior Analysis Code & Custom Bonsai workflows for virtual shoaling setup	This paper	https://bitbucket.org/mpinbaierlab/larschandbaier2018
NetLogo 6.0.2	[33]	https://ccl.northwestern.edu/netlogo/
Bonsai 2.3.1	[50]	https://bonsai-rx.org/
FFMPEG	NA	https://www.ffmpeg.org/
Anaconda Python	Anaconda, Inc.	https://conda.io
Prism 7.04	graphpad	https://www.graphpad.com
idTracker	[51]	http://www.idtracker.es/
Other		
Projection film	Rosco	Tough Rolux 3000
Watch glass	Duran group	Cat# 233214607
Cameras	IDS, PointGrey	UI-3370CP-NIR, Grashopper GS3-U3-41C6NIR-C
16 mm Lens	Edmund Optics	Cat# 86-571
25 mm Lens	Edmund Optics	Cat# 86-572
Projector	Optoma	ML750ST
IR illumination	Solarox	IR1-60-850
280 × 340 mm custom cold mirror	Praezisions Glas & Optik, Germany	custom made
White Light LED	Lumitronix	Multibar 35
IR band pass filter	Edmund Optics	Cat# 84-802

CONTACT FOR REAGENT AND RESOURCE SHARING

Further information and requests for resources and reagents should be directed to and will be fulfilled by the Lead Contact, Herwig Baier (hbaier@neuro.mpg.de).

EXPERIMENTAL MODEL AND SUBJECT DETAILS

Wild-type designates the strain Tupfel Longfin (TL). For our experiments, we used progeny of random matings from multiple groups of three male and three female TL adults. Eggs were collected and raised in Danieau's solution (17 mM NaCl, 2 mM KCl, 0.12 mM MgSO4, 1.8 mM Ca(NO3)2, 1.5 mM HEPES) in groups of 25 larvae. At 5 dpf, larvae were transferred to 3 L Techniplast tanks containing system water. Larvae were fed dry food (Sera Micron) three times per day until 20 dpf, supplemented with live rotifer culture once per day. Artemia culture was supplemented starting at 21dpf. Animals were kept at 27.5°C on a 14h/10h light/dark cycle with the lights turning on at 7 am. Despite this tight control of rearing conditions, animals of the same clutch sometimes varied by a factor of three in body size (data not shown) and we used animals approximately belonging to the second and third quartiles of body size judging by eye. For the experiment in Figure 2E, we sorted individual eggs in Danieau's solution into the wells of 12 well plates (Corning Costar). Visual contact between wells was blocked by folding white paper strips between the wells. At 5dpf, the larvae were transferred to 1 L tanks and otherwise treated and fed the same way as group housed animals. Visual contact between tanks was blocked at all times by white paper towels.

On the day of the experiment, animals were transferred to experimental dishes filled with system water using a cut disposable pipette for animals younger than 16 dpf or a sieve for older animals. Once in the setup, experiments were typically started within

15 min. Setup water temperature ranged from 21 to 24°C. Since gonadal differentiation has not occurred at this stage, males and females were used indiscriminately. All animal procedures conformed to the institutional guidelines of the Max Planck Society and the local government (Regierung von Oberbayern). After the experiment, animals were euthanized by an overdose of Tricaine followed by immersion in ice cold water.

METHOD DETAILS

In summary, we built a setup to record the position of up to 15 individual zebrafish simultaneously in real-time and project arbitrary, animal-centric visual stimuli onto a screen below the animals (Figure S1E). Animals were monitored in shallow glass dishes of 10 cm diameter (Duran group, watch glass, nr. 233214607) filled with system water until 1 mm below the inner rim (10 mm height, 40 mL). A custom built grid was laser cut from 3 mm opaque acrylic and positioned to prevent visual contact between dishes. The dishes rested on a projection film (Rosco Tough Rolux 3000 or Rosco Rolux 400) for visual stimulation. In this arrangement, distance of the fish's eyes from the screen was confined to approximately between 3 mm and 13 mm by the rounded bottom of the dish and the surface of the water. To limit stimulus distortion due to refraction at the air-glass-water interfaces, we submerged the projection film and glass dishes in a 400 × 600 × 100 (width/length/height) tray custom built from a 5 mm glass bottom and 10 mm acrylic walls. The water in the tray reached up to 1 mm below their outer rim of the dishes to prevent animals from escaping. Animals were recorded at 30 fps with cameras using the CMV4000 sCMOS chip (IDS UI-3370CP-NIR or PointGrey Grashopper GS3-U3-41C6NIR-C) at a resolution of 2048x1280 pixels. For virtual interactions, we used a 16 mm lens (Edmund Optics Nr. 86-571) at a distance of 850 mm resulting in an image resolution of 268 um/px to record 15 individual animals simultaneously using one camera. To record up to 8 physically interacting pairs, we used two cameras at a resolution of 2048x2048 pixels each and 25 mm lenses (Edmund Optics Nr. 86-572) at a distance of 500 mm resulting in an image resolution of 100 um/px. Visual stimuli were generated from a projector (Optoma ML750ST) reflected onto the projection film from underneath via a 280 × 340 mm custom cold mirror (Praezisions Glas & Optik, Germany). Infrared illumination was generated from six hundred SMD 3528 LEDs (850 nm) arranged on strips (Solarox LED strips IR1-60-850) over an area of 900 × 600 mm and passed through a diffusing sheet of frosted acrylic and the cold mirror before reaching the animals. Visible light was provided by the projector with the exception of the experiment in Figure S1B where we used white light LED strips (Multibar 35 LED strip, Lumitronix) for reliable switching in an otherwise completely dark room. Illumination was computer controlled using 5V relay switches (Adafruit) driven by an Arduino. For experiments with visual stimulation, visible light to the camera was blocked by an IR band pass filter (Edmund Optics Nr. 84-802). Image acquisition at 30 fps, real-time processing and stimulus generation was performed on a Desktop PC (Intel Xeon E5-1630, 16GB RAM) running Bonsai [50]. Briefly, each camera frame was background subtracted and a threshold was applied to isolate animals against the background. Next, contours were extracted to compute center of mass and orientation of each animal.

Based on animal positions and an optional stimulus position file, we populated the projector frame via openGL drawing routines. A pairing matrix defined which animals were virtually linked during specified episodes of an experiment. Stimuli were black dots (RGB value (0,0,0)) on white background (RGB value (255,255,255)) unless noted otherwise. Dot size was a multiple of projected pixel size (1 px was 0.47 mm side length). Constant speed paths in Figures 2A and 2B were generated in two steps: First, we selected the path of a single 24 dpf animal that was previously recorded during physical interaction. This 'natural' path was interpolated by a factor of 100. Next, a search algorithm walked along the interpolated path to select successive equidistant points. The distance was selected to match the average speed of the original path. Intermittent motion was generated by displacing the stimulus dot along a synthetic knot shaped path at defined time intervals instantaneously to a new position. The knot shape was used as a locally smooth path that includes slow changes in direction of path curvature. Its shape is defined by the Lissajous curve (sin(2t),cos(3t), $0 < t < 2pi$). In between position updates, the dot was stationary. For experiments shown in Figures 2C–2E average speed was 5.7 mm/sec for all conditions. For experiments shown in Figures 2F and 2G, dot speed was modulated by sub-sampling the interpolated path at appropriate step sizes. The dot position update interval for intermittent motion in Figure 2F was 666 ms. Constant motion designates a position update interval of 33 ms. Animal and stimulus parameters were streamed to a text file for offline analysis. The program also stored the video data after background subtraction into an xVid compressed .avi file via ffmpeg (ffmpeg.org) for later inspection.

Camera and projector were aligned using a separate Bonsai routine once per day: With the IR pass filter removed from the camera, we recorded the position of four reference points projected onto the projection film to compute the perspective transformation from camera to projector pixel coordinates using the openCV function *getPerspectiveTransform*. Animals swimming at a distance from the projection screen are detected with a lateral offset on the camera frame relative to the orthogonal axis of the projection screen (Figure S1F). We corrected for this effect by transforming animal coordinates from camera coordinates to projection screen coordinates depending on the offset from the camera's optical axis, assuming an average distance of 10 mm of the animals from the projection screen and applying intercept theorem. Physical interactions in Figure 1 and Figure S1 were tracked offline using idTracker [51]. To improve its performance with videos of uneven infrared illumination, we pre-processed videos applying a divisive background correction: A python script generated a median projection frame from ten randomly picked frames of the video. We used ffmpeg to divide each frame of the video by this median frame.

QUANTIFICATION AND STATISTICAL ANALYSIS

Output files were analyzed offline using custom written Python scripts. Briefly, we first assigned each animal to a pair, either with another animal or with a dot stimulus to quantify inter animal distance (IAD) or animal dot distance, respectively. Next, we obtained a distribution of control IAD by time shifting the position time series of one animal versus the other for 10 times. This represents the expected IAD based on chance encounters in the absence of attraction [20]. To quantify attraction, we computed the percent reduction in mean observed IAD relative to the mean of 10 mean shuffled control IAD_s during a period of 5 min unless otherwise noted:

$$Attraction = \frac{IAD_{shuffled} - IAD_{observed}}{IAD_{shuffled}}$$

In some experiments, we noticed that attraction was low during the initial 5-15 min, potentially reflecting stress related effects of the sudden changes of the environment, water temperature and light levels upon transfer into the setup (data not shown). We therefore excluded the first presentation of each stimulus (typically 30-45 min) of data at the beginning of each experiment from the analysis except for Figure 1D. Individual experiments lasted up to 12 hours (Figure 1D) but were typically limited to 6 repetitions of each 5 min stimulus condition.

The statistical unit to report the spread of repeated-measurements is 1 standard deviation (SD) over individual animals throughout all figures unless otherwise noted. For experiments involving multiple repetitions of several stimulus conditions, the mean across repetitions was obtained for each animal before computing SD across animals.

To provide an intuition for the spread of repeated-measurements of attraction, we used control data to compute the 95% confidence interval (CI) that represents a null hypothesis of no attraction. For this, we analyzed attraction during 5 min chunks of time shifted pairs: Each chunk of real data was time shifted 10 times by different durations. Next, one shifted chunk was picked to compute IAD whereas the remaining 9 chunks were used to compute a mean control IADs. This is analogous to the procedure for real data. Analysis of attraction between virtually linked pairs during periods when no stimulus was visible yielded similar results (Figure S1C). The 95% CI was approximated as a range of 4 standard deviations around the mean of the distribution of control attraction. Animals were identified as significantly attracted if attraction exceeded the 95%CI of the null hypothesis.

To analyze the effect of recording duration on the spread of repeated-measurements of attraction, we used the same data and concatenated individual 5 min chunks of IAD time series to compute control attraction for various simulated recording durations. Figure S1D shows how the CI predictably depends on the duration of the recording. We therefore re-computed the 95% CI for all data plots to reflect the shortest data duration that was available for any of the animals plotted in a given figure panel.

For Figure 2B, group differences were statistically analyzed using PRISM 7.04. Each animal was exposed to all stimuli but note that for the mutual interaction condition, pairs of animals were analyzed together, yielding only one data point per two animals. We therefore limited our matched samples 1-Way ANOVA (non-parametric Friedman test) and Dunn's post hoc test for multiple comparisons to the four passive stimuli.

To determine maxima of stimulus tuning curves we first averaged repeated trials recorded for each animal. Next, the maximum was identified from this average tuning curve for each animal. We excluded animals in which the maximum attraction was less than 0.05. Similar results were obtained by including all animals. Attempts to interpolate the measurements were abandoned. To quantify correlations between two sets of data, we used linear least-squares regression implemented in the function *linregress* of SciPy. The outputs include R: correlation coefficient and p: two-sided p value for a hypothesis test that the slope of the fit is zero. Error bands in panels 1D and 4BC represent 95 percent confidence intervals obtained by bootstrapping as part of the plotting function *tsplot* of Seaborn 0.8.1.

Neighborhood maps were computed inspired by previous work [16]. Briefly, 2 hour position time series of each animal were smoothed using a hamming filter with a width of 5 frames (160 ms) before calculating animal heading as the direction of motion. Each animal was used as a focal animal to calculate relative position of its neighbor. Next, the time series of relative positions were rotated around the focal animal by its instantaneous heading at each time point. We then plotted 2D histograms of rotated relative neighbor positions in 1 square mm bins, revealing the probability of finding the neighbor at a specific place. The values are normalized such that all bins have a value of 1 when neighbor density is evenly distributed. Maps of individual animals were averaged using the mean operation. Swim bouts were identified using a custom peak detection algorithm on time series of instantaneous swim speed derived from the smoothed position time series. To analyze attraction in quartets (Figure 5BC) we separately calculated attraction between the six possible pairs and averaged the four values corresponding to small-large pairings.

To analyze animal separation at stimulus transitions (Figure 3), we first calculated average time series of dot animal distance during each stimulus type for each animal. The experiment consists of 6 min segments for each stimulus condition. The test transition of stimulus attractiveness lasts 90 s. The timing of the transition relative to the beginning of a 6 min segment was randomized within a window of 60 to 120 s after the beginning of a segment to minimize effects of occasional local dish occupancy biases of individual fish. The data were aligned with respect to the transition before averaging the trials of each animal. Next, we normalized the average I-C-I and I-X-I time series to a range from 0 to 1 by subtracting at all time points the IAD value at the last frame before the first stimulus transition and dividing by the 90th percentile of the resulting series. To limit this analysis to animals reliably attracted to the stimulus we excluded 16 out of 30 animals whose average normalized IAD time series went below a value of -1 at any point during the I-C-I or I-X-I condition. The dissociation slope was calculated as a linear fit through 10 s of the normalized IAD time series after stimulus transition for each animal using the function *linregress* of SciPy. Slopes were compared using matched samples t test.

Multi-agent Model

The virtual arena was modeled as a circle of 100 mm diameter. Agents moved at constant speed of 0.2 mm per simulated time step, resulting in an agent swim speed of 6 mm per 30 frames, closely matching our experimental conditions where animals are recorded at 30 frames per second and swim on average at 3-7 mm/sec (Figure 2G). At the boundary of the virtual arena, agents reversed into a random direction until pointing away from the boundary.

Avoidance of collisions was not explicitly modeled and within the 100 mm virtual arena, all agents were visible to each other. At every turn event (every 30 steps), IAD was calculated and saved for post hoc analysis of attraction produced by the model.

To simulate the effect of individual's social drive on mutual attraction (Figure 4E), we repeatedly ran the model for 72,000 steps (40 min simulated time) using different sets of p_{s1} and p_{s2} for two agents, respectively. For each run of the model, agents were initially positioned randomly and mean IAD over the model run was saved for subsequent analysis. Each parameter combination was tested 120 times. Attraction was calculated analogous to the real data, using as control IAD the outcome of the model when both p_{s1} and p_{s2} were set to zero. Each set was simulated six times for 9,000 steps, corresponding to 6 repeated trials of 5 min each for the pairwise combinations in Figure 4B.

To demonstrate that our model can produce assortative shoaling, we explicitly implemented a factor σ for self-preference. This parameter acts directly to bias social turns toward animals of the same group. To achieve this, the centers of mass of each animal were weighted by this factor according to which group they belong and social turns were directed toward the weighted average center of mass.

For 4 agents belonging to two types, the weighted average was computed as follows:

σ: self-preference ($0 < \sigma < 1$)
S: self-type agent
O_1 and O_2: other type agents

$$Weighted\ average = S\left(\frac{1}{3}+\frac{2}{3}\sigma\right) + O_1\left(\frac{1}{3}-\frac{1}{3}\sigma\right) + O_2\left(\frac{1}{3}-\frac{1}{3}\sigma\right)$$

For $\sigma = 0$ (no self-preference), this model is equivalent to the simple model described above where agents turn toward the average center of mass for all animals.

For $\sigma = 1$ (complete self-preference), agents only consider their own type without any contribution from other types to the average center of mass.

In this model, self-preference of 0.5 or higher reproduced the observed suppression of between-type attraction (Figure S5A).

DATA AND SOFTWARE AVAILABILITY

Raw behavior data is available at FigShare: (https://doi.org/10.6084/m9.figshare.6939923). Custom python code for data analysis from raw data to final figures and custom Bonsai workflows for virtual shoaling setup are accessible on Bitbucket: (https://bitbucket.org/mpinbaierlab/larschandbaier2018).

Current Biology, Volume *28*

Supplemental Information

Biological Motion as an Innate Perceptual Mechanism Driving Social Affiliation

Johannes Larsch and Herwig Baier

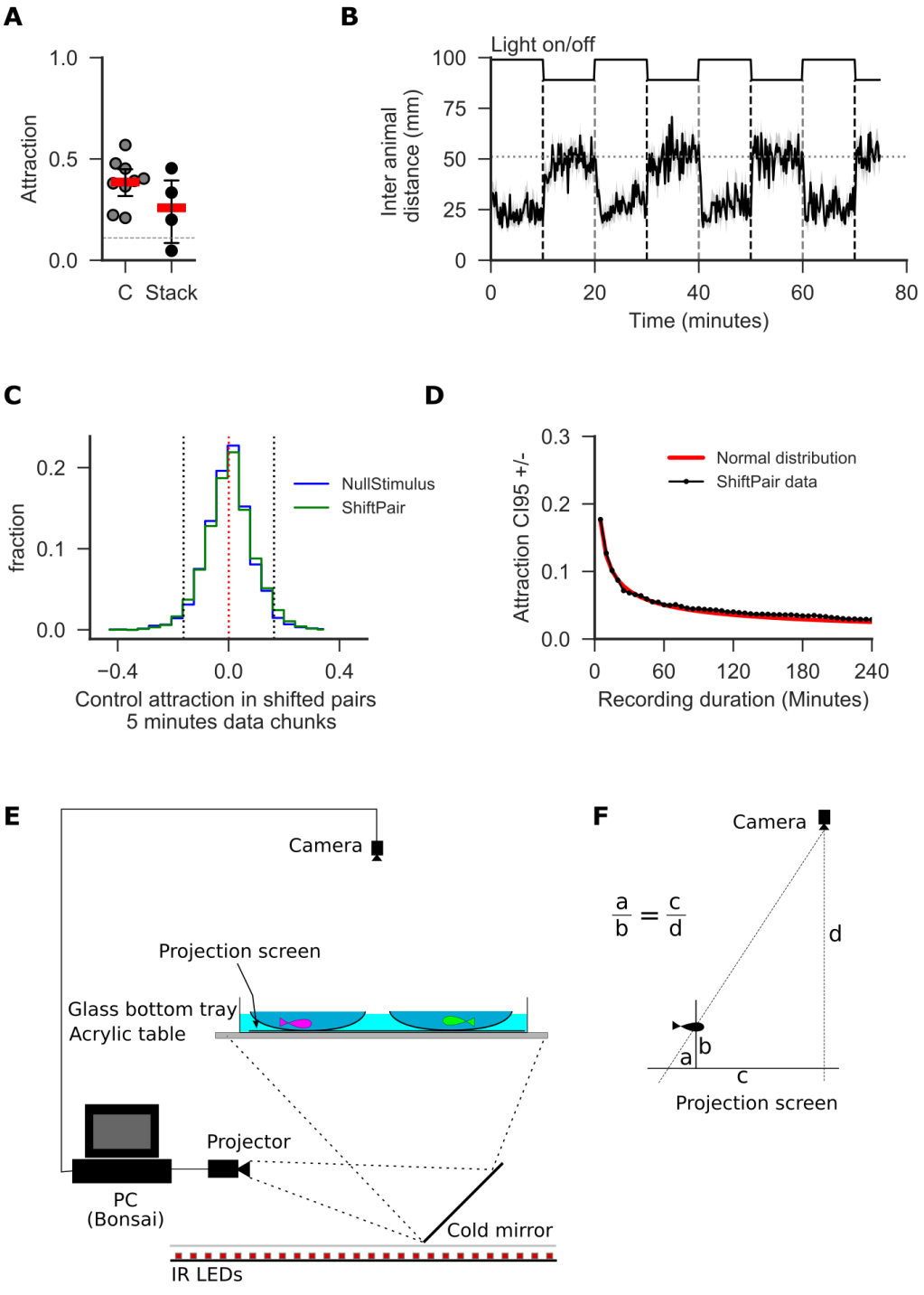

Figure S1: Visual sensory input can induce and is indispensable for social attraction. Related to Figure 1. (A) Animals swimming physically separated in vertically stacked transparent 10 cm

dishes are still attracted to one another. C: Control pairs without physical barrier. Data points represent mutual attraction of individual pairs over a 1 hour period. Red bars indicate mean. Error bars represent 1 SD. Dashed line: 95% confidence interval (CI) for h_0 of no attraction. **(B)** Inter animal distance (IAD) quickly approached chance level (dotted line) when lights were turned off and returned to a low steady state when lights were turned back on. Animals were physically interacting as pairs in glass dishes. Black line indicates mean IAD of 6 pairs, binned in 10 second intervals. Gray shading indicates 95% CI. **(C)** Distribution of attraction during 5 minute chunks of data when no stimulus was shown (blue) and for time shifted pairs (green) provides an estimate of the spread of repeated measurements of attraction. Dotted lines: mean (red) and 95% CI (4 SD, black). Data is the same as in Figure 1E. **(D)** 95% CI narrows with longer data recording. Black dots represent 2 SD of distributions of attraction in time shifted pairs during bins of increasing duration. First data point corresponds to the distribution in (C). The data is approximated by dividing the CI value for attraction in one time bin by the square root of the number of time bins (red) as expected from a normal distribution. Same data as (C). **(E)** Schematic of the virtual shoaling setup. **(F)** Lateral offset of the apparent animal position relative to axis orthogonal to projection plane is corrected by applying intercept theorem. b is approximated to 10 mm. d is 850 mm. c is the lateral offset of the animal from the vertical camera axis.

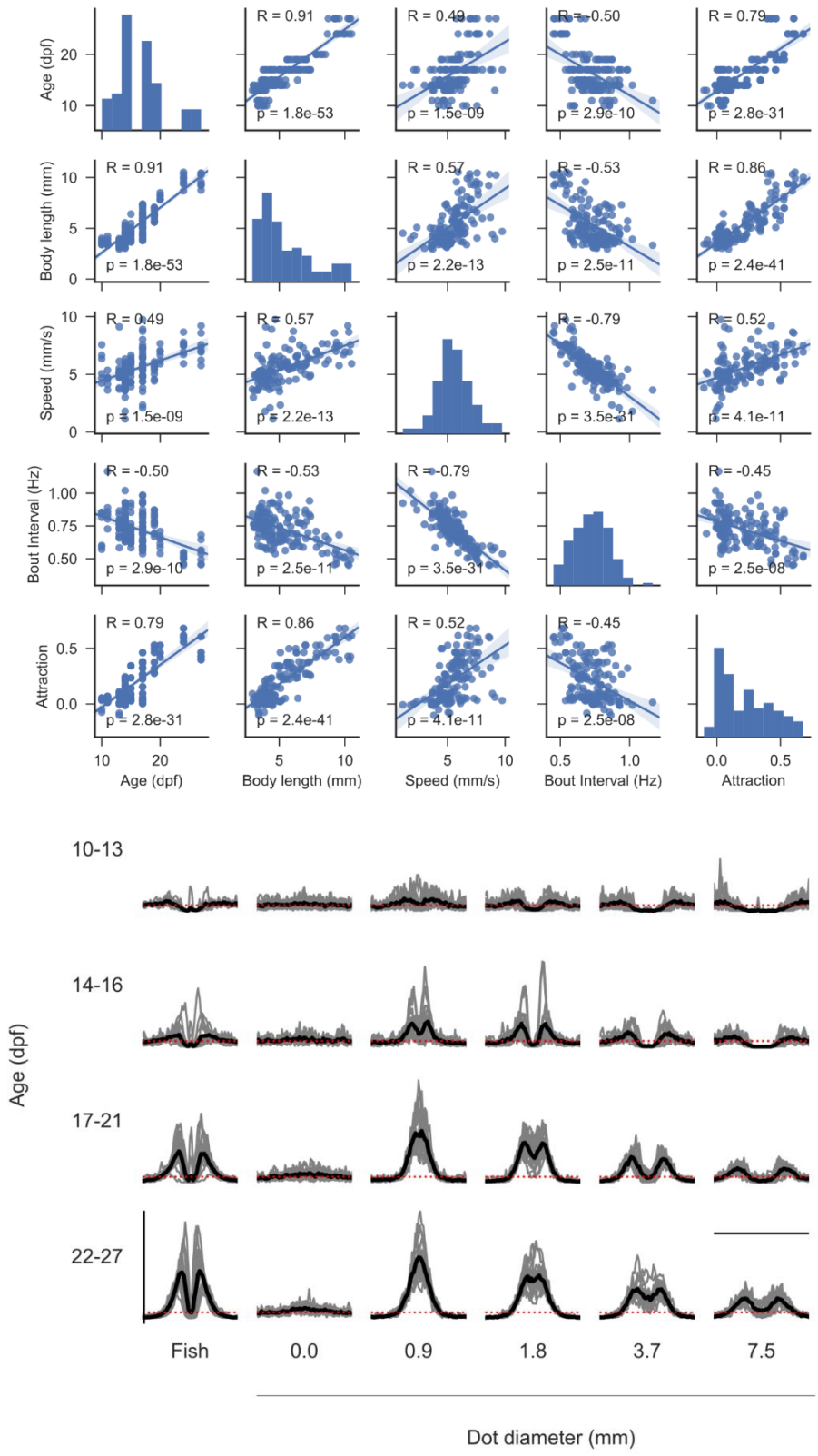

Figure S2: Development of swim kinetics and neighbor interactions, related to Figure 1. (**Top**) Interdependence of age, body length, average swim speed, bout interval and attraction during

virtual reciprocal interactions via 3.7 mm live dots. Same data as Figure 1E. (**Bottom**) Intensity profiles through the central horizontal 3 mm band of neighborhood plots in Figure 1G. Note the short range avoidance at the center of profiles corresponding to highly attractive stimuli (compare Figure 1F). Red dotted line indicates neighbor density expected at chance. Gray lines represent individual animals, black lines represent mean over all animals. Horizontal scale bar represents 60 mm. Vertical scale bar represents a 20-fold increase in neighbor density relative to chance levels (analogous to neighborhood maps in Figure 1G). Same data as Figure 1G.

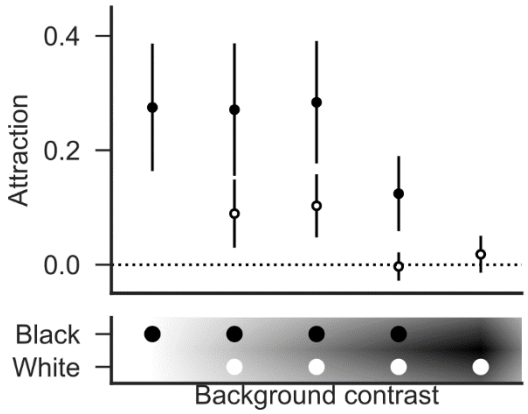

Figure S3: Dark on light but not light on dark dot contrast is attractive. Related to Figure 2. Data points represent mean +/- 1SD, n=15 animals. Projector RGB values for dots and background were 0%, 25%, 50%, 75% and 100% of (255,255,255), respectively.

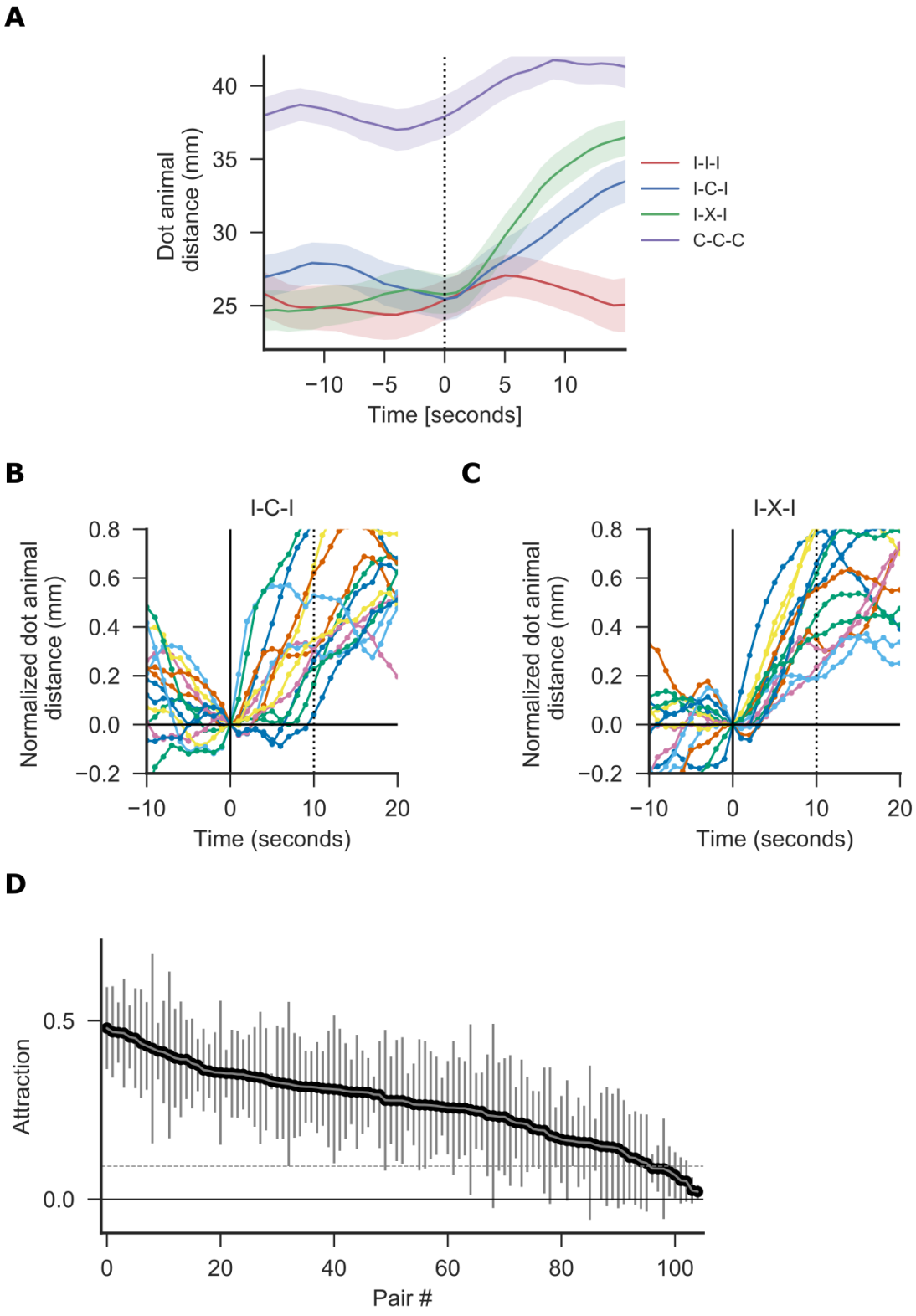

Figure S4: Dot-animal separation after stimulus transition and attraction for individual pairs, related to Figure 3 and Figure 4. (A) Rapid increase in dot animal distance upon stimulus

transition. Same data as Figure 3B, zoomed into the 30 second time window around stimulus transition occurring at t = 0 seconds. Traces represent mean +/- 95% confidence interval. Inflection in ICI and IXI traces is noticeable in less than 5 seconds. Overlap of CI on traces for I-C-I and I-X-I transitions with I-I-I ends within 5-10 seconds. **(B,C)** Individual animal normalized dot animal distance around stimulus transitions I-C-I and I-X-I occurring at t = 0 seconds. Data represent mean distance over 20 trials per condition. Colors indicate animals across stimulus conditions. Same data as Figure 3C,D. Slopes in Figure 3D represent the slope of a linear fit through 10 seconds of data after the transition. Similar results were obtained using 5 seconds of data. **(D)** Repeatability of attraction during sequential virtual interactions via interactive dots in Figure 4B. Data represent mean attraction +/- 1 SD. N = 6 repeated trials for each of the 105 possible pair permutations of 15 animals. Dashed line represents 95% CI. Same Data as in Figure 4B.

A

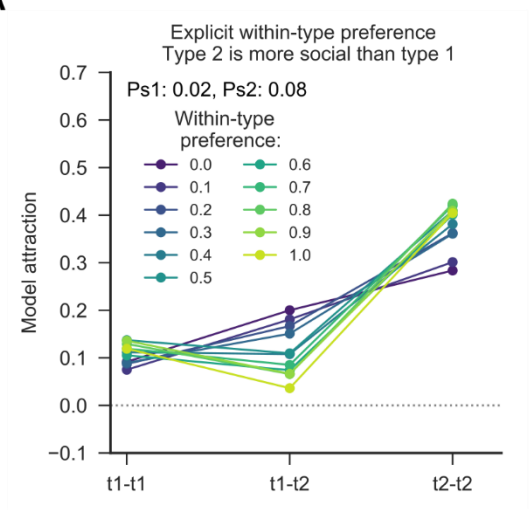
Explicit within-type preference
Type 2 is more social than type 1
Ps1: 0.02, Ps2: 0.08
Within-type preference:
0.0
0.1
0.2
0.3
0.4
0.5
0.6
0.7
0.8
0.9
1.0
Model attraction
0.7
0.6
0.5
0.4
0.3
0.2
0.1
0.0
−0.1
t1-t1
t1-t2
t2-t2

B

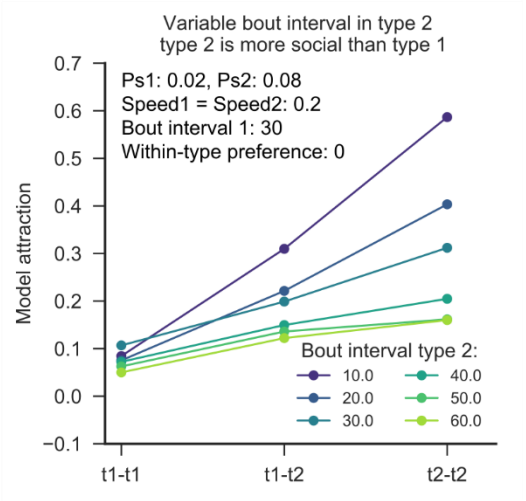
Variable bout interval in type 2
type 2 is more social than type 1
Ps1: 0.02, Ps2: 0.08
Speed1 = Speed2: 0.2
Bout interval 1: 30
Within-type preference: 0
Bout interval type 2:
10.0
20.0
30.0
40.0
50.0
60.0
Model attraction
0.7
0.6
0.5
0.4
0.3
0.2
0.1
0.0
−0.1
t1-t1
t1-t2
t2-t2

C

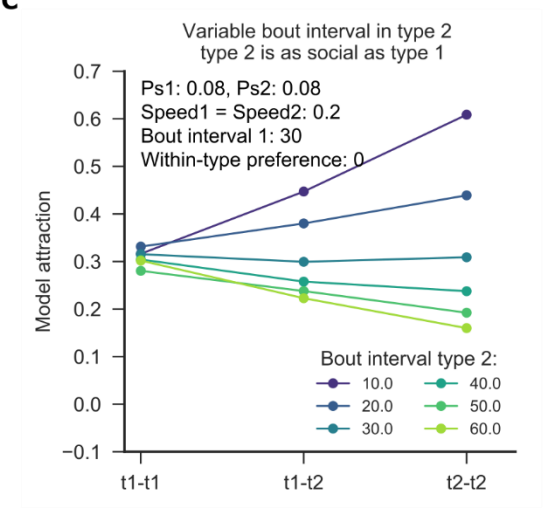
Variable bout interval in type 2
type 2 is as social as type 1
Ps1: 0.08, Ps2: 0.08
Speed1 = Speed2: 0.2
Bout interval 1: 30
Within-type preference: 0
Bout interval type 2:
10.0
20.0
30.0
40.0
50.0
60.0
Model attraction
0.7
0.6
0.5
0.4
0.3
0.2
0.1
0.0
−0.1
t1-t1
t1-t2
t2-t2

D

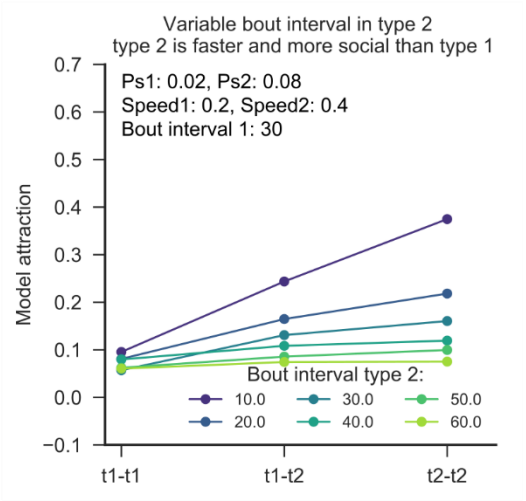
Variable bout interval in type 2
type 2 is faster and more social than type 1
Ps1: 0.02, Ps2: 0.08
Speed1: 0.2, Speed2: 0.4
Bout interval 1: 30
Bout interval type 2:
10.0
20.0
30.0
40.0
50.0
60.0
Model attraction
0.7
0.6
0.5
0.4
0.3
0.2
0.1
0.0
−0.1
t1-t1
t1-t2
t2-t2

E

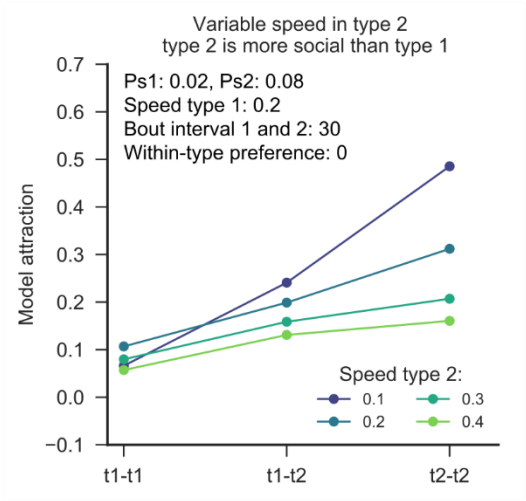
Variable speed in type 2
type 2 is more social than type 1
Ps1: 0.02, Ps2: 0.08
Speed type 1: 0.2
Bout interval 1 and 2: 30
Within-type preference: 0
Speed type 2:
0.1
0.2
0.3
0.4
Model attraction
0.7
0.6
0.5
0.4
0.3
0.2
0.1
0.0
−0.1
t1-t1
t1-t2
t2-t2

Figure S5: Active self-preference but not differences in bout rate or swim speed between agent types explain assortative shoaling in the multi agent model. Related to Figure 5. (A) Within-type preference weights agents according to group membership for social turns towards the center of mass of all agents. Higher preference gives more weight to the agent of the own type. **(B)** Bout interval alone was modulated in the more social type. **(C)** Case where both types are equally social (Ps1=Ps2) and equally fast. Bout rate was modulated in type 2. **(D)** Combined effects of differences in speed and bout interval. As in real animals, the more social type (older animals) swims faster by a factor of 2. **(E)** Speed alone was modulated in the more social type. In all cases presented here except (A: within-group preference), attraction between types is equal to or higher than the mean of attraction within types.

1-Way ANOVA

Friedman test	
P value	<0.0001
Exact or approximate P value?	Approximate
P value summary	****
Are means signif. different? (P < 0.05)	Yes
Number of groups	4
Friedman statistic	67.07
Data summary	
Number of treatments (columns)	4
Number of subjects (rows)	38

Multiple Comparisons

Number of families	1
Number of comparisons per family	6
Alpha	0.05

Dunn's multiple comparisons test	Rank sum diff.	Significant?	Summary	Adjusted P Value
natPath_natBout vs. natPath_constSpeed	64	Yes	****	<0.0001
natPath_natBout vs. syntPath_natBout	22	No	ns	0.3037
natPath_natBout vs. syntPath_constSpeed	82	Yes	****	<0.0001
natPath_constSpeed vs. syntPath_natBout	-42	Yes	**	0.0011
natPath_constSpeed vs. syntPath_constSpeed	18	No	ns	0.6585
syntPath_natBout vs. syntPath_constSpeed	60	Yes	****	<0.0001

Table S1: Post-hoc multiple comparisons related to Figure 2B.